VARIATION IN THE H_3^+ EMISSION OF URANUS

Hoanh An Lam,[1,2] Steven Miller,[1,2] Robert D. Joseph,[3] Thomas R. Geballe,[4] Laurence M. Trafton,[5]
Jonathan Tennyson,[1] and Gilda E. Ballester[6]

ABSTRACT

Infrared images of Uranus, obtained in 1993 April, at wavelengths sensitive to the H_3^+ molecular ion, are presented. These show that spatial variation in the emission from the planet is discernible. Comparison with magnetic field modeling of Uranus indicates that sources of this variation may include auroral activity and other features, but the images show that the spatial variation is more limited than in the case of Jupiter. This conclusion is born out by spectra obtained on four consecutive nights during 1995 June, which show that the overall temporal variability of the H_3^+ emission is ~20%. Comparison of the 1995 June spectra with data obtained in 1992, and the 1993 images, shows that the overall brightness of H_3^+ emission of Uranus can vary by a factor of 2 on a timescale of years.

Subject headings: atmospheric effects — infrared: solar system — planets and satellites: individual (Uranus)

1. INTRODUCTION

The detection of the fundamental ($\nu_2 \rightarrow 0$) spectrum of the H_3^+ molecular ion on Uranus by Trafton et al. (1993) opened up the possibility of comparative studies of the ionospheric properties of the outer planets using this molecular ion as a probe. H_3^+ has been studied on Jupiter since its first identification in the Jovian auroral zones by Drossart et al. (1989), and, shortly after the 1993 Uranus detection, a weak spectrum of H_3^+ was detected on Saturn (Geballe, Jagod, & Oka 1993).

The spectrum of Uranus obtained by Trafton et al. (1993) had a spectral resolution of 1100 and a spatial resolution of $3''.1 \times 3''.1$. Since the apparent diameter of Uranus at that time was $3''.57$, there was effectively no spatial resolution of the planet. A planetwide total H_3^+ emission of 5×10^{11} W was reported, obtained by combining the derived temperature (740 K) and column density (6.5×10^{10} cm^{-2}) with a temperature versus total emission/molecule curve based on the data of Kao et al. (1991).

On Jupiter, particle precipitation is mainly responsible for the auroral H_3^+ emission (Drossart et al. 1989), while a combination of this mechanism and photoionization is invoked to explain the weaker low-latitude emission due to this ion (Lam 1995). *Voyager* ultraviolet measurements showed the Uranian aurorae to be relatively weak (Broadfoot et al. 1986; Herbert & Sandel 1991), and solar extreme-ultraviolet was put forward as the main source of excitation (Strobel et al. 1991). Trafton et al. (1993) had insufficient spatial resolution to determine whether their measured H_3^+ emission was associated with the auroral regions of Uranus (located around the magnetic poles)—and therefore due mainly to particle precipitation—or with emission due to photoionization.

In this Letter, we present images of Uranus obtained at wavelengths sensitive to H_3^+ obtained in 1993 and *L*-window (3.4–4.1 μm) moderate-resolution spectra obtained in 1995 that, taken together, show that there is spatial variation in the Uranian emission level of this ion. To our knowledge, our 1993 images (first presented at the AAS Division of Planetary Sciences meeting in 1993; Lam et al. 1993) are the first *L*-window images of this planet and some of very few at any wavelength which show features.

2. OBSERVING PROCEDURE

Images of Uranus were obtained on 1993 April 22 and 23 using the then facility infrared camera (ProtoCAM) on the NASA Infrared Telescope Facility (IRTF) on Mauna Kea, Hawaii. The planet was imaged at 3.533 and 3.986 μm, wavelengths chosen to maximize the H_3^+ emission, and at 3.80 μm, where H_3^+ emission is relatively weak. A stare/nod-to-sky observing mode was employed, with nods approximately every 60 s. An observing log is given in Table 1. Tracking was maintained by guiding on a nearby star and was accurate to $\pm 0''.25$. Overall tracking and seeing effects gave rise to a smearing of $0''.75$ full width at half-maximum. Broadband *J* images (centred on 1.2 μm) were also obtained to assist with the location of the planet on the array. Absolute calibration of the images was obtained using HD 106965 as a ratio star.

Spectra of Uranus were obtained on 1995 June 11–14 at the United Kingdom Infrared Telescope (UKIRT) using the facility long-slit spectrometer CGS4 at a plate scale of $1''.23$. A 75 line mm^{-1} grating and 1 pixel–wide slit aligned east-west were employed to cover the wavelength range 3.47–4.13 μm, which includes key transitions in the H_3^+ ν_2 fundamental band. The spectrometer setup gave a spectral resolving power of $\lambda/\Delta\lambda \sim 1400$ at the center of our wavelength range. The observing log for these observations is also in Table 1. Spectra were taken in a stare-nod mode, using a nod of 10 array rows along the slit direction. Seeing and tracking errors gave a smearing of about $1''$ full width at half-maximum. BS 7205, an F5 star, was used for ratioing and flux calibration. A list of observed lines and intensities is given in the Appendix as Table 4.

In 1993 April, Uranus subtended $3''.57$. The sub-Earth

[1] Department of Physics and Astronomy, University College London, Gower Street, London WC1E 6BT, England.
[2] Visiting Astronomer at the NASA Infrared Telescope Facility, which is managed and operated for NASA by the University of Hawaii Institute of Astronomy.
[3] Institute for Astronomy, 2860 Woodlawn Drive, Honolulu, HI 96822.
[4] Joint Astronomy Centre, 660 N. A'ohoku Place, Hilo, HI 96720.
[5] McDonald Observatory and Department of Astronomy, University of Texas at Austin, Austin, TX 78712.
[6] Department of Atmospheric, Oceanic and Space Sciences, University of Michigan, 2455 Hayward, Ann Arbor, MI 48109.

TABLE 1
Observing Log for 1993 Images and 1995 Spectra

Date	Central Time (UT)	Wavelength (μm)	Integration Time (s)
1993 Apr 22....	13:30	3.533	1800
	14:30	3.986	1500
	15:20	3.800	480
1993 Apr 23....	13:00	3.986	1800
	14:10	3.533	1200
	15:00	3.800	600
1995 Jun 11	12:13	3.800	270
1995 Jun 12	12:52	3.800	285
1995 Jun 13	12:30	3.800	390
1995 Jun 14	11:54	3.800	150

TABLE 2
Quadrant-averaged H_3^+ Emission Levels at 3.986 Millimeters

	E (3.986 μm)$/W \times 10^{-16}$ m^{-2}	
QUADRANT	April 22	April 23
1	0.79 ± 0.08	0.63 ± 0.06
2	0.60 ± 0.06	0.67 ± 0.07
3	0.43 ± 0.06	0.45 ± 0.06
4	0.69 ± 0.06	0.52 ± 0.06
Total	2.51 ± 0.13	2.27 ± 0.12

latitude was −57°, and the polar position angle was 274°. This meant that the southern rotational pole was located 1″.02 from the limb of the planet. In 1995 June, the diameter of Uranus subtended 3″.70. The sub-Earth latitude was −49°, and the polar position angle was 270°. The northern magnetic pole is located at latitude −15° and, given the planet's rotation period of 17.24 ± 0.01 hr, must have been visible on at least one of the observing nights for both sets of observations. However, the uncertainty in the rotation period is sufficient that the position of the magnetic poles, located at the time of *Voyager 2*, cannot be ascertained.

3. RESULTS

3.1. *Images*

Figure 1 (Plate L11) shows the *L*-window images, after flat-fielding, removing bad pixels, and applying a median 3×3 filter. While Uranus is clearly visible at $\lambda = 3.986$ μm and fairly so at $\lambda = 3.533$ μm, the $\lambda = 3.80$ μm image shows no sign of the planet. At $\lambda = 3.986$ μm, 75% of the pixels covering the planet had signal-to-noise (S/N) ratios of 2 or better; peak intensities gave S/N of 8. Even allowing for the shorter integration time, the S/N ratio per pixel of the $\lambda = 3.80$ μm image relative to $\lambda = 3.986$ μm should have been 0.57 on April 22 and 0.58 on April 23, everything else being equal. Thus, Uranus should have been clearly detectable had the intensity at this wavelength been the same at $\lambda = 3.986$ μm. To test this further, we added one-third of the frame intensity at 3.986 μm to the 3.80 μm. The result, indeed, was that the planet was clearly visible.

The detection of the planet at H_3^+ wavelengths—at $\lambda = 3.533$ μm and, even more clearly, at $\lambda = 3.986$ μm—but not at the relative H_3^+ null of $\lambda = 3.80$ μm—demonstrates that the images obtained were sensitive to emission from this ion rather than reflected solar infrared [or the effect of the known "red leak" of the ProtoCAM circular variable filter (CVF); R. D. Baron, private communication]. Analysis of the spectrum of Trafton et al. (1993) supports this conclusion; in their spectrum, the background intensity was just a few percent of the peaks. The intensity of the image at $\lambda = 3.986$ μm was $2.51(\pm 0.13) \times 10^{-16}$ W m^{-2}, averaged over the planet, on April 22, and $2.27(\pm 0.12) \times 10^{-16}$ W m^{-2} on April 23. Convolving the 1992 spectrum at this wavelength (Trafton et al. 1993) with the CVF profile gives $2.31(\pm 0.12) \times 10^{-16}$ W m^{-2}, in good agreement with the images, strengthening the conclusion that the images were genuinely mapping the H_3^+ intensity distribution.

To assist with further analysis, a planetary spheroid was fitted to the images. For the April 23 images, this could be reliably fixed using the offset between the negative beam, which fortuitously included a bright star and the *J*-window image for guidance. For April 22, the fit was less reliable, making use of the *J*-window image and adjusting the position of the spheroid by a few pixels to encompass as much of the bright emission as possible. In addition, the planet was arbitrarily divided into four quadrants by axes running north-south and east-west on the sky. Starting in the top left (northeast) and running clockwise to finish in the bottom left (southeast), the quadrants were labeled 1 to 4. Figure 2 (Plate L12) shows the spheroid fitted images at 3.533 and 3.986 μm for April 22 and 23. Quadrant-averaged emissions at 3.986 mm, the clearer of the two wavelengths, are given in Table 2.

The images show that the H_3^+ emission was not distributed evenly across the planet but had significant structure to it. In particular, there was an extensive, bright region in the April 22 3.986 mm image in quadrant 1, with a secondary bright region mainly in quadrant 4. On April 23, the brightest region was in quadrant 2. The table confirms this impression of nonuniformity and indicates that, despite the uncertainty in the derived emission levels, local diurnal variations occurred in quadrants 1 and 4, where the values for the 2 days do not overlap. The total emission from the planet, however, remained essentially constant.

3.2. *Spectra*

At the time of our observations, Uranus spanned three rows of the CSG4 detector. These were co-added and analyzed as one spectrum. This process improved the signal-to-noise ratio but led to the loss of spatial information as to the distribution of the Uranian H_3^+ emission. The spectra obtained during 1995 June 11–14 were analyzed using the technique described in Trafton et al. (1993), with additional improvements due to Lam (1995). These workers derived H_3^+ temperatures, $T(H_3^+)$, and column densities, $\rho(H_3^+)$, from fits to the Kao et al. (1991) data set and subsequent additions. But these parameters are highly anticorrelated in the fitting, and Lam et al. (1996) have introduced a parameter $E(H_3^+)$, the total H_3^+ emission, combining the temperature and column density under the assumption that the ion's emitting levels are rotationally thermalized.

The fitted spectra for the three nights are shown in Figure 3, and the accompanying derived parameters are shown in Table 3. The average fitted temperature for the planet over the four nights was 677 K (± 40 K), slightly cooler than that obtained by Trafton et al. (1993), but with an overlapping range. Temperatures and column densities showed some variation, with the June 11 and June 14 values of $T(H_3^+)$ being higher than for the intervening 2 days. Although June 11 appears to represent a minimum in the fitted column density, the variation in $E(H_3^+)$ is more significant in view of the known (anti-)correlation in fitting $T(H_3^+)/\rho(H_3^+)$ pairs. The data suggest that, after being
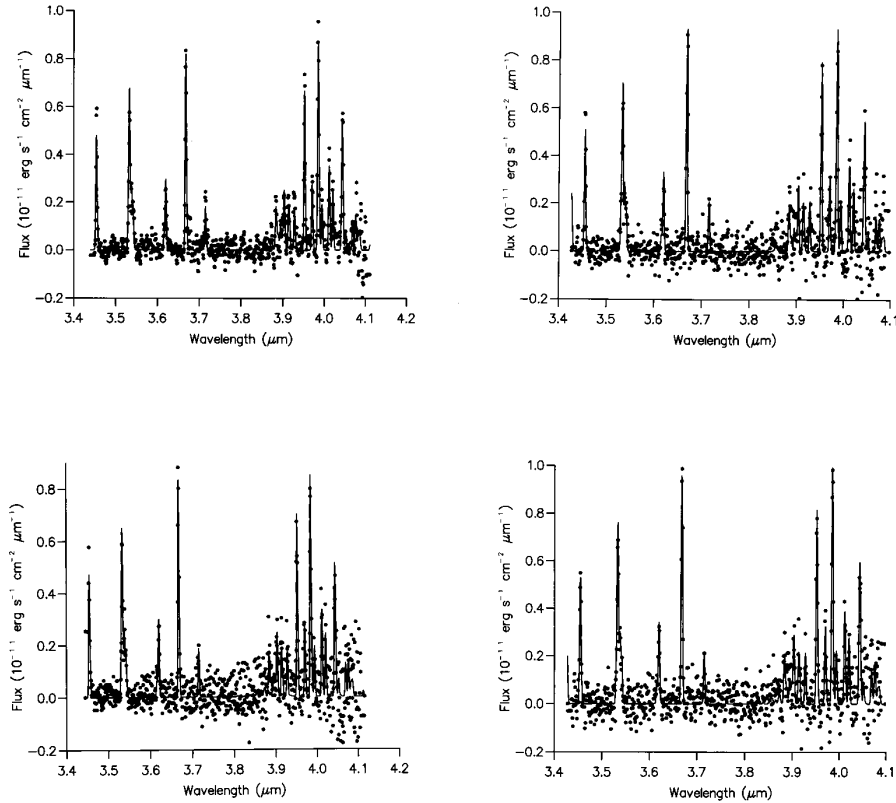
FIG. 3.—Fitted CGS4 spectra of Uranus from 1995. *Top left*: June 11; *top right*: June 12; *bottom left*: June 13; *bottom right*: June 14. *Filled circles*: observed spectrum; *solid line*: fitted spectrum.

virtually constant for two nights, the total emission fell by 10% between June 12 and 13 before rising again by about 20% on June 14. However, the values obtained for all the parameters fall within each other's ranges of uncertainty.

4. DISCUSSION

The detection of spatial variation in the H$_3^+$ images of Uranus raises the question as to the source of this variation. In magnetic models of Uranus (Connerney, Acuna, & Ness 1987; Hudson, Clarke, & Warren 1989; Herbert & Sandel 1991), the auroral region visible from Earth is confined inside the Miranda footprint, around the north magnetic pole, itself located at a latitude of S15°. This is shown by the heavily dotted area in Figure 4. Since the polar position angle was 274° in 1993 and 270° in 1995, the north magnetic pole ought to have been visible from Earth ~60% of the time on both occasions. Auroral regions are associated with enhanced particle precipitation and thus higher levels of H$_3^+$ emission. The rotation of the planet would have advanced the auroral region clockwise through the quadrants on subsequent (terrestrial)

TABLE 3

FITTED PARAMETERS FOR 1995 JUNE CGS4 SPECTRA OF URANUS

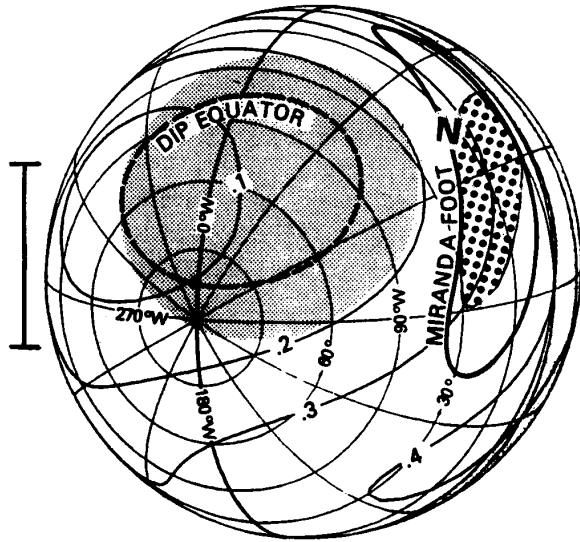| Date (UT)	T(H$_3^+$) (K)	ρ(H$_3^+$) (10^{14} m^{-2})	E(H$_3^+$) (μW m^{-2})
11 ...	700 ± 70	4.3 ± 0.5	14.9 ± 1.5
12 ...	663 ± 70	5.8 ± 0.6	14.6 ± 1.5
13 ...	664 ± 70	5.3 ± 0.5	13.3 ± 1.5
14 ...	680 ± 70	5.7 ± 0.6	16.1 ± 1.6

days, possibly explaining the shift in the brightest quadrant from quadrant 1 (April 22) to quadrant 2 (April 23).

There is also a region close to the southern rotational pole of Uranus, known as the Dayside Polar Anomaly (DPA) (Hudson et al. 1989), where the magnetic field is weak. This is shown in Figure 4 as the lightly dotted area. This can also be a region of high particle precipitation (R. Prangé, private communication). This region might therefore also have higher than planet-average H$_3^+$ emission levels. If the auroral region had been located in quadrant 1 on April 22, as we suggest above, the DPA would have been in quadrant 4, moving mainly into quadrant 1 on April 23. The distribution of emission given in Table 2 is consistent with this behavior.

The spectra obtained in 1995, however, set fairly strict limits on the level of overall variation that auroral activity (coupled with any contribution the DPA might add) can make. With a 1″.23 slit set along the planetary central meridian longitude and the 0″.75 smearing due to observing conditions, the combined spectra were averages over at least 50% of the planet. Given the timing of the observations, it is highly unlikely that the auroral region was never in the slit. Depending on the uncertainty in the measurements, the E(H$_3^+$) values obtained could be interpreted if the auroral region were located in quadrant 2 on June 11 (partly in the slit), in quadrant 3 on June 12 (partly in the slit), behind the planetary disk on June 13, and in quadrant 1 on June 14 (fully in the slit). (N.B.: this scenario is meant to be indicative; the data are insufficient to say if it truly represents the behavior of Uranus during the observations.)

This would set a reasonable limit to the increase in H$_3^+$ emission due to auroral activity to $2.8^{+3.1}_{-2.8}$ μW m^{-2} averaged

FIG. 4.—Aspect of Uranus as seen from Earth in 1993. *Heavy dots*: auroral region; *light dots*: Dayside Polar Anomoly; N: north magnetic pole; vertical bar I: position and width of the UKIRT slit in 1995; *heavy contours*: magnetic field strengths (G) (after Hudson et al. 1989).

over (50% of) the dayside planetary disk, an increase of just over 20% if the June 13 value is taken to indicate a total absence of auroral activity. (N.B.: the uncertainty in the results mentioned previously means that all the spectral measurements lie within each other's uncertainty ranges.) Recent studies of Jupiter (Ballester et al. 1994), by comparison, show that under the same observing conditions, the presence of auroral activity on the Jovian scale would increase the planet-averaged emission by a factor of ∼5 compared with spectra obtained when no aurorae were in view.

Finally, if the temperature and column density obtained for the 1995 spectra were representative of the whole planet, then the total H_3^+ emission would have been roughly 50% of that of 1992 and 1993, indicating temporal variability on the longer timescale (∼3% of a Uranian year). Only 20% of this decrease is accountable for by a drop in H_3^+ column density. The main part is due to the apparently lower temperatures derived.

5. CONCLUSIONS

At present, while the limited nature of the spatial variation of H_3^+ emission from Uranus is clear, the interpretation is much less so. The present data set is too restricted, and it will require further imaging and/or spectroscopic observations before the various factors effecting the Uranian H_3^+ emission can be reliably pinned down. Nonetheless, this study does show that H_3^+ studies of Uranus may have an important future—as with the case of Jupiter—in enabling us to understand the complex magnetic and ionospheric properties of this intriguing planet. One interesting feature of Uranus, in comparison with Jupiter, is that auroral activity appears to play a far less significant role in the production of H_3^+. Emission seems to be dominated by a planetwide H_3^+ glow.

APPENDIX

This appendix contains a list of observed lines and intensities in Table 4.

TABLE 4

H_3^+ LINE EMISSION FROM URANUS

Observed Wavelength (μm)	Flux (10^{-17} W m^{-2})	Peak S/N	Identification	Laboratory Wavelength (μm)	Observed Wavelength (μm)	Flux (10^{-17} W m^{-2})	Peak S/N	Identification	Laboratory Wavelength (μm)
3.454	2.3	27	$5,3,-1 \to 4,3$	3.455	3.994	0.8	4	$3,2,-1 \to 3,2$	3.995
			$5,4,-1 \to 4,4$	3.455	4.013	1.8	9	$4,1,-1 \to 4,1$	4.012
3.534	2.3	28	$4,3,-1 \to 3,3$	3.534				$4,2,-1 \to 4,2$	4.013
3.619	1.5	12	$3,2,-1 \to 2,2$	3.620	4.021	1.1	4	$4,3,-1 \to 4,3$	4.022
3.670	3.4	40	$2,1,+1 \to 1,1$	3.668	4.045	2.0	7	$5,2,-1 \to 5,2$	4.043
			$2,0,+1 \to 1,0$	3.669				$5,3,-1 \to 5,3$	4.044
3.715	0.8	8	$2,1,-1 \to 1,1$	3.715				$5,1,-1 \to 5,1$	4.045
3.891	1.1	8	$5,5,+1 \to 5,5$	3.889				$5,0,-1 \to 5,0$	4.045
3.903	1.1	8	$3,3,+1 \to 3,3$	3.904	4.070	0.9	3	$0,1,+1 \to 1,1$	4.070
3.915	1.0	7	$2,2,+1 \to 2,2$	3.915	4.082	1.0	2	$6,4,-1 \to 6,4$	4.076
3.928	0.9	7	$1,1,+1 \to 1,1$	3.929				$6,3,-1 \to 6,3$	4.077
3.953	2.8	22	$1,0,-1 \to 1,0$	3.953				$6,2,-1 \to 6,2$	4.082
3.971	1.3	10	$2,1,-1 \to 2,1$	3.971				$6,1,-1 \to 6,1$	4.085
3.985	3.1	25	$3,0,-1 \to 3,0$	3.986				$6,5,-1 \to 6,5$	4.087
			$3,1,-1 \to 3,1$	3.987					

REFERENCES

Ballester, G. E., Miller, S., Tennyson, J., Trafton, L. M., & Geballe, T. R. 1994, Icarus, 107, 189
Broadfoot, A. L., et al. 1986, Science, 233, 89
Connerney, J. E. P., Acuna, M. H., & Ness, N. F. 1987, J. Geophys. Res., 92, 15239
Drossart, P., et al. 1989, Nature, 340, 539
Geballe, T. R., Jagod, M.-F., & Oka, T. 1993, ApJ, 410, L109
Herbert, F., & Sandel, B. R. 1991, BAAS, 1147
Hudson, M. K., Clarke, J., & Warren, J. A. 1989, J. Geophys. Res., 94, 6517
Kao, L., Oka, T., Miller, S., & Tennyson, J. 1991, ApJS, 77, 317

Lam, H. A. 1995, Ph.D. thesis, Univ. of London
Lam, H. A., Achilleos, N., Miller, S., Tennyson, J., Trafton, L. M., Geballe, T. R., & Ballester, G. E. 1996, Icarus, submitted
Lam, H. A., Miller, S., Joseph, R. D., & Tennyson, J. 1993, BAAS, 25, 1080
Strobel, D. F., Shemansky, D. E., Yelle, R. V., & Atreya, S. K. 1991, in Uranus, ed. J. T. Bergstrahl, E. D. Miner, & M. S. Matthews (Tucson: Univ. Arizona Press), 65
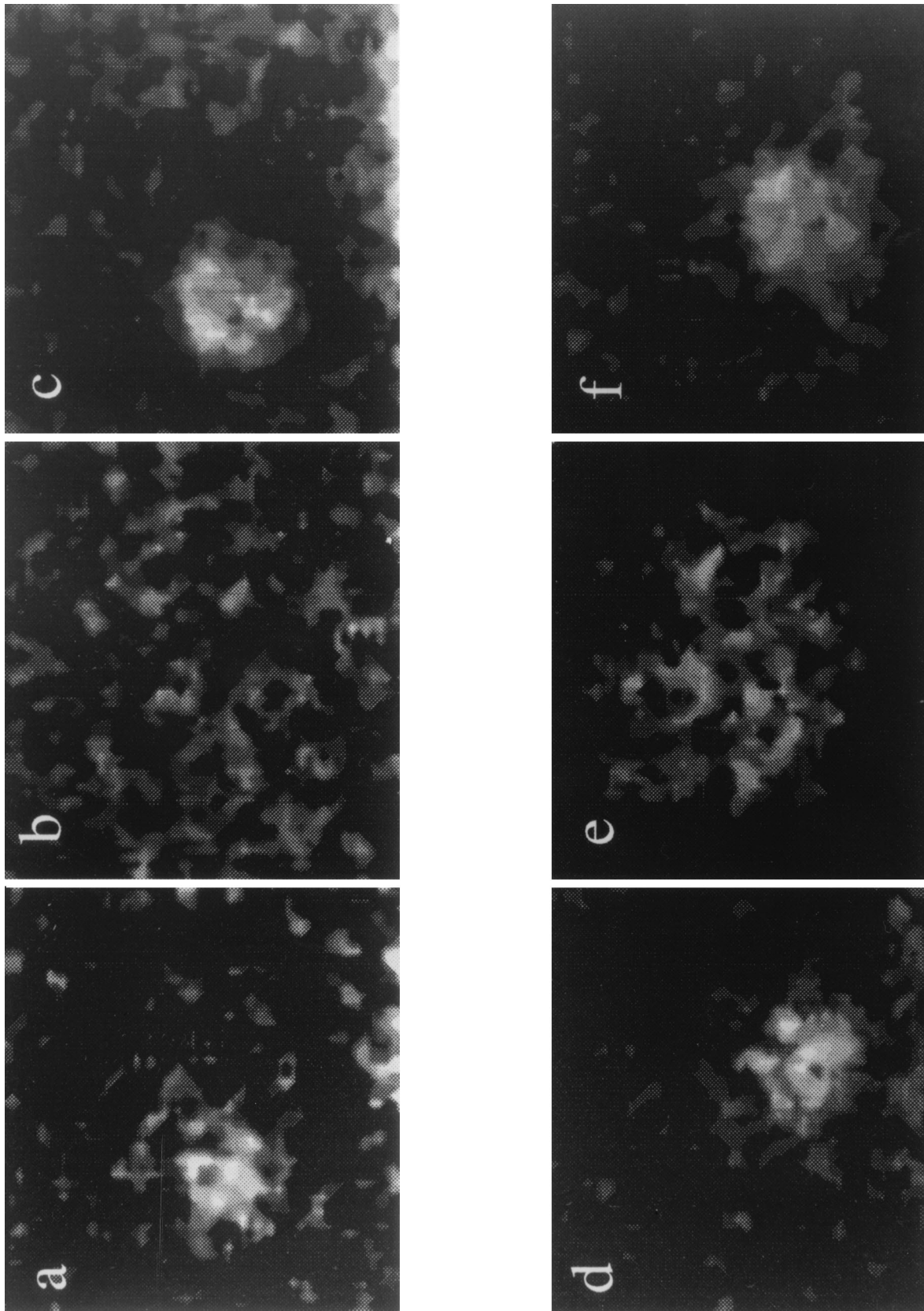Trafton, L. M., Geballe, T. R., Miller, S., Tennyson, J., & Ballester, G. E. 1993, ApJ, 405, 761

FIG. 1.—Infrared images of Uranus taken in 1993. *Top row*: April 22 (*a*) λ = 3.533 μm, (*b*) λ = 3.80 μm, (*c*) λ = 3.986 μm. *Bottom row*: April 23 (*d*) λ = 3.533 μm, (*e*) λ = 3.80 μm, (*f*) λ = 3.986 μm.
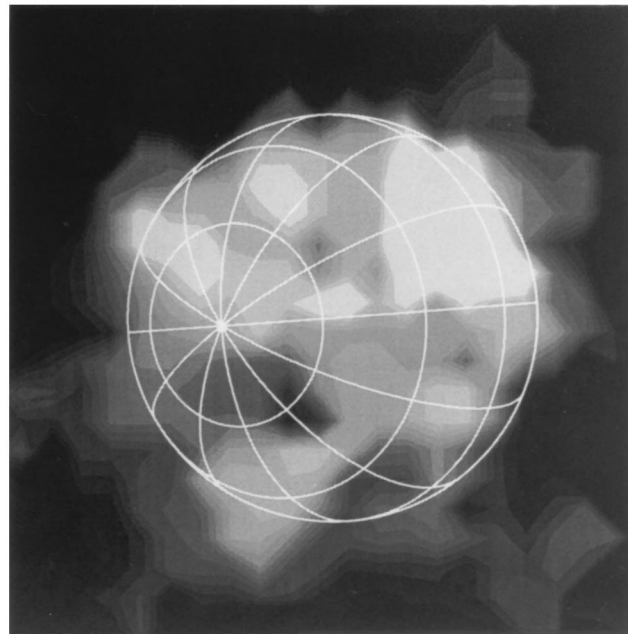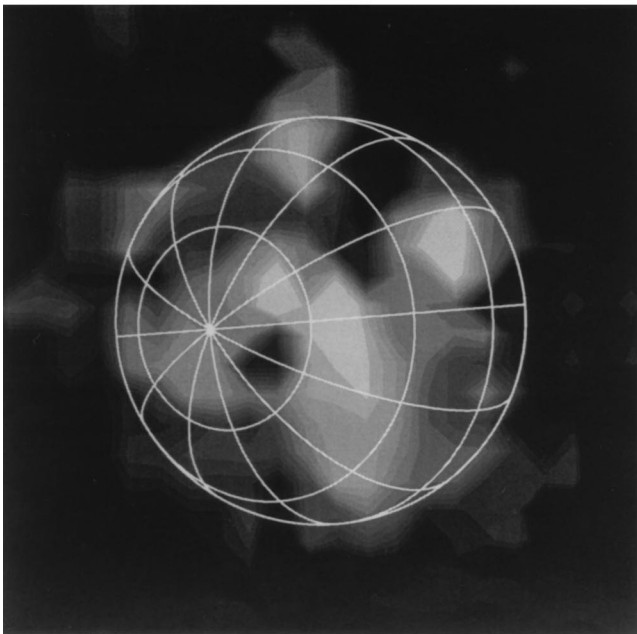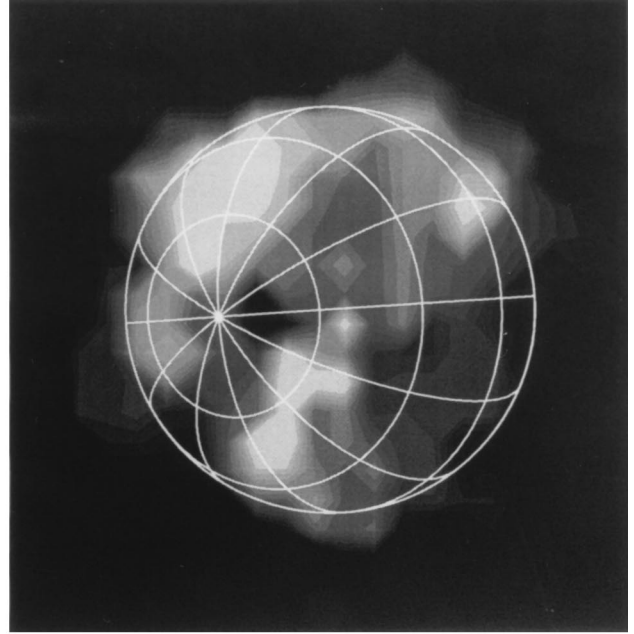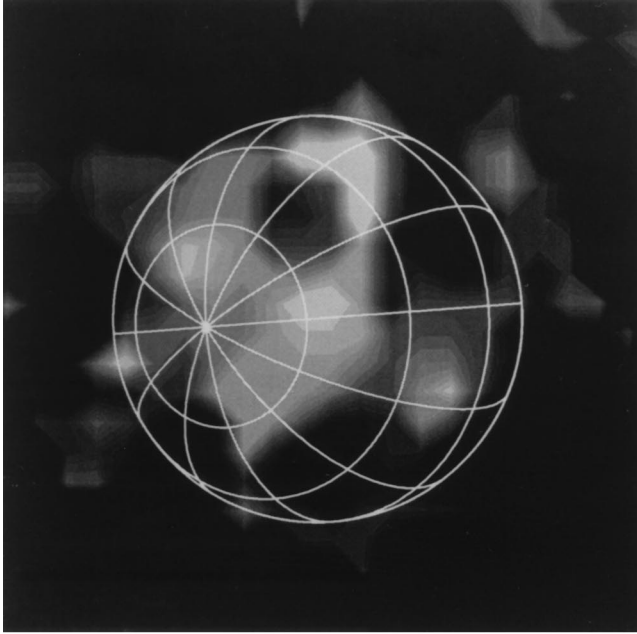
LAM et al. (see 474, L74)

Fig. 2.—Images at $\lambda = 3.533$ μm and $\lambda = 3.986$ μm fitted with planetary spheroid. *Top row*: April 22; *bottom row*: April 23.